PAPER

Solute–solute correlations responsible for the prepeak in structure factors of undercooled Al-rich liquids: a molecular dynamics study

IOP Publishing Journal of Physics: Condensed Matter
J. Phys.: Condens. Matter **27** (2015) 205701 (7pp) doi:10.1088/0953-8984/27/20/205701

Solute–solute correlations responsible for the prepeak in structure factors of undercooled Al-rich liquids: a molecular dynamics study

Feng Zhang[1], Yang Sun[1,2], Zhuo Ye[1], Yue Zhang[1], Cai-Zhuang Wang[1,3], Mikhail I Mendelev[1], Ryan T Ott[1], Matthew J Kramer[1,4], Ze-Jun Ding[2] and Kai-Ming Ho[1,3]

[1] Ames Laboratory, US Department of Energy, Ames, IA 50011, USA
[2] Hefei National Laboratory for Physical Sciences at Microscale and Department of Physics, University of Science and Technology of China, Hefei, Anhui 230026, People's Republic of China
[3] Department of Physics and Astronomy, Iowa State University, Ames, IA 50011, USA
[4] Department of Materials Science and Engineering, Iowa State University, Ames, IA 50011, USA

E-mail: fzhang@ameslab.gov

Received 5 February 2015, revised 25 March 2015
Accepted for publication 7 April 2015
Published 6 May 2015

Abstract

We have performed molecular dynamics simulations on a typical Al-based alloy $Al_{90}Sm_{10}$. The short-range and medium-range correlations of the system are reliably produced by *ab initio* calculations, whereas the long-range correlations are obtained with the assistance of a semi-empirical potential well-fitted to *ab initio* data. Our calculations show that a prepeak in the structure factor of this system emerges well above the melting temperature, and the intensity of the prepeak increases with increasing undercooling of the liquid. These results are in agreement with x-ray diffraction experiments. The interplay between the short-range order of the system originating from the large affinity between Al and Sm atoms, and the intrinsic repulsion between Sm atoms gives rise to a stronger correlation in the second peak than the first peak in the Sm–Sm partial pair correlation function (PPCF), which in turn produces the prepeak in the structure factor.

Keywords: metallic liquids, structure factor, molecular dynamics, prepeak

(Some figures may appear in colour only in the online journal)

1. Introduction

A group of new materials formed by Al and 10–15 at.% rare earths (REs) and/or transition metals (TMs) have attracted considerable interest in recent decades [1]. These materials can sustain deep undercooling during rapid quenching, even though the concentration of the primary element Al is as high as 90 at.%. Many members of this group can form glass with the desired large strength-to-weight ratio [1]. In addition, nanocrystalline composite materials can be formed through carefully designed rapid solidification and devitrification processes [1–6]. These composite materials are characterized by fine crystalline phases dispersed in an amorphous or glassy matrix, and they often display further improved mechanical properties. A satisfactory knowledge of the structure of deeply undercooled Al–RE liquids is fundamental not only to understanding the glass formation but also to understanding and controlling phase selection during the crystallization process. The Al–Sm binary alloy chosen for this study is a representative member of Al–RE alloys. It is of particular interest because it offers the widest glass-forming composition range in the Al–RE series [1] and an array of stable and metastable crystalline phases that are attainable from the liquid or the glass, including fcc, a big cubic phase,

Al_5Sm, Al_4Sm, and $Al_{11}Sm_3$, which have all been observed experimentally [2, 7, 8].

Although there is no long-range periodicity, short-range to medium-range structural order exists in undercooled metallic liquids or glasses [9]. Understanding and controlling the underlying atomic order with various degrees of undercooling that results in this resistance to crystallization for metals has been a challenge in materials science for more than 50 years [10]. X-ray and neutron diffraction are widely used techniques to probe the structural properties of these materials. For a large set of Al-based amorphous alloys, the total structure factor $S(q)$ measured in the diffraction experiments displays a unique feature, that is, there exists a distinct prepeak before the major peak [11–17]. Such prepeak has been extensively studied on covalent or ionic glasses and liquids [18–24]. In these systems, the short-range order (SRO) is usually well-defined by a simple polyhedron (such as tetrahedron in SiO_2 glass), and the networking of such polyhedrons can give rise to the prepeak located at smaller q than the position of the primary peak in the total structure factor. In metallic systems, however, the lack of a universal building block substantially increases the difficulty of relating the subtle prepeak in the reciprocal space to the real-space correlations. Some previous work that tried to establish this mapping was mainly speculative. For example, Hsieh *et al* suggested that the prepeak in Al–Fe–Ce alloys is originated from certain icosahedral ordering because the prepeak is in close vicinity to a diffraction peak of icosahedral quasicrystal Al–Fe [11]. Recently, the reverse Monte Carlo (RMC) method, which generates atomic structures by directly fitting to experimental diffraction data, has been used to model Al-based amorphous alloys [14–17]. Although the RMC method provides useful insights, it is inconclusive in most cases because of multi-fold limitations of this method: it often leads to multiple qualitatively different solutions; the resulting atomic structures cannot sustain energetic relaxation; and it can result in overfitting, i.e. fitting to experimental error or noise.

In this article, we perform *ab initio* molecular dynamics (AIMD) simulations on a typical Al-based system, $Al_{90}Sm_{10}$, to capture the short-range to medium-range correlations of the system. The long-range correlations are then obtained by classical molecular dynamics (CMD) using a semi-empirical potential well-fitted to *ab initio* data. Our results successfully show the prepeak in the total structure factor, suggesting that the simulations have captured the essential structural ordering that is responsible for the prepeak.

2. Methods

In this section, we describe the AIMD procedure and the calculation of the structure factor. Details about CMD are deferred to the next section.

The AIMD simulations are performed within the density functional theory (DFT), as implemented in the VASP package [25]. The projected augmented-wave (PAW) method [26] is used to describe the electron–ion interaction, and the generalized gradient approximation (GGA) in the Predew–Burke–Ernzerhof (PBE) form [27] is used for the exchange-correlation energy function. A cut-off energy of 240 eV is used for the plane-wave basis. The constant number of atoms, volume, and temperature (*NVT*) ensemble is applied with Nose–Hoover thermostats [28]. The Verlet algorithm is used to integrate Newton's equation of motion, using a time step of 3 fs. The unit cell contains 500 atoms, with 450 Al and the remaining are Sm. To prepare the samples, a randomly generated structure is first melted and equilibrated at 2100 K over 2000 time steps. Then, the sample is cooled to 800 K, which is well-below the melting temperature for $Al_{90}Sm_{10}$ 1200 K [29], with a cooling rate of 2.2×10^{13} K s^{-1}. The cooling procedure in AIMD is separated into a series of sequential jobs. In each job, the temperature is reduced by 10 K in 150 steps. The final atomic positions, velocities, and the charge density of the previous job are used to initiate the new job, with the box size reduced by 7.7×10^{-3} Å, a value predetermined by monitoring the pressure of the cell during the cooling process. After that, the structures at 1300, 1000, and 800 K are collected separately for further isothermal annealing for approximately 6000 time steps. The first 3000 time steps are not used in the analysis to ensure equilibrium has been reached.

The total structure factors $S(q)$ from the MD simulations are calculated by the Faber–Ziman formalism [30]:

$$S(q) = \omega_{11} S_{11}(q) + \omega_{12} S_{12}(q) + \omega_{22} S_{22}(q). \tag{1}$$

In equation (1), the subscripts 1 and 2 refer to Al and Sm species, respectively. The weight factors $\omega_{\alpha\beta}$ are determined by the molar fraction of the species x_1 andx_2, as well as the q-dependent atomic form factors $f_1(q)$ and $f_2(q)$ [31]:

$$\omega_{11} = \frac{x_1^2 f_1^2(q)}{[x_1 f_1(q) + x_2 f_2(q)]^2}, \tag{2}$$

$$\omega_{12} = \frac{2x_1 x_2 f_1(q) f_2(q)}{[x_1 f_1(q) + x_2 f_2(q)]^2}, \tag{3}$$

and

$$\omega_{22} = \frac{x_2^2 f_2^2(q)}{[x_1 f_1(q) + x_2 f_2(q)]^2}. \tag{4}$$

$S_{\alpha\beta}(q)$ are the partial structure factors, which are related to the partial pair-correlation functions (PPCFs) $g_{\alpha\beta}(r)$ by

$$S_{\alpha\beta}(q) = 1 + 4\pi\rho_0 \int_0^\infty r^2 \frac{\sin qr}{qr} \left[g_{\alpha\beta}(r) - 1\right] \mathrm{d}r, \tag{5}$$

where ρ_0 is the atomic density of the liquids.

3. Results and discussions

We start by comparing the AIMD structure factors with the experimental data. It should be taken into account that the AIMD has two limitations. The first limitation is associated with very short simulation time, which allows a system to reach an equilibrium structure only at rather high temperatures. Therefore, it is reasonable to compare the AIMD results with the experiment at the highest temperature available in experiment. The second limitation is that the model size in

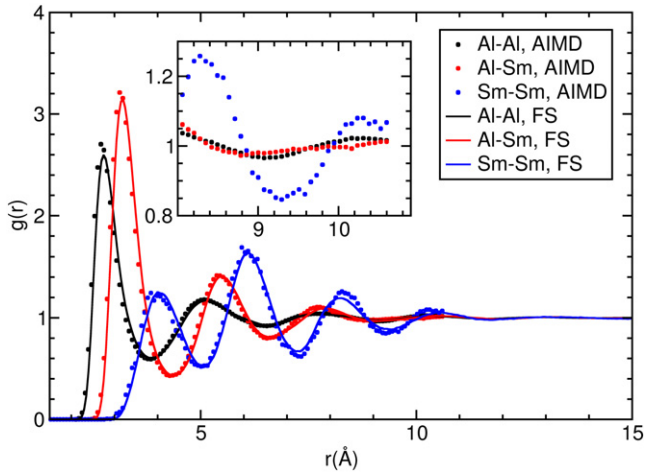

Figure 1. The PPCFs of $Al_{90}Sm_{10}$ liquid at 1300 K, calculated by AIMD (solid circles) and FS potential fitted to *ab initio* data (solid lines). The inset zooms-in the PPCFs near the cut-off radius (10.61 Å) from AIMD calculations.

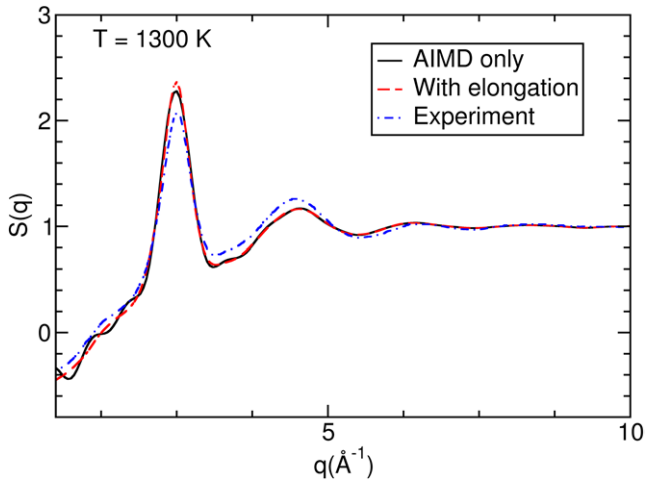

Figure 2. Total structure factor of the $Al_{90}Sm_{10}$ liquid at $T = 1300$ K, calculated by only AIMD and AIMD with the elongation method. The structure factor obtained in x-ray diffraction experiments at the same temperature is also shown.

AIMD is usually not large enough to capture the long range correlations in the system. This can be seen in figure 1, where the dots show the PPCFs of the liquid sample calculated at $T = 1300$ K. The PPCFs are terminated at $r = 10.61$ Å, which is half of the size of the simulation box (a). Although our system with 500 atoms/unit cell already approaches the limit that AIMD can handle based on current computational capabilities, the PPCFs fail to fully converge to unity at the cutoff radius a / 2, especially for the Sm–Sm pair correlations $g_{22}(r)$. This premature convergence creates noticeable noises, typically in the form of oscillating ripples [32], in the short-q region of $S(q)$ calculated according to equation (5). The solid black line in figure 2 gives the total $S(q)$ at 1300 K calculated based on AIMD results, where one can see such noises in the short-q region, which cause qualitative disagreement with the experimental values (dashed–dotted blue line) [33]. To correct it, one has to extend the model size so that correlations of longer range can be included. Ideally, this should be done by increasing the unit cell size in the AIMD simulations, which creates unfeasibly high computational cost. However, the correlations at short to medium range and at longer range are not independent. On the contrary, the latter is largely determined by the former. Therefore, if one can train an efficient semi-empirical potential to reproduce the short to medium range correlations that can be reliably obtained in AIMD calculations, then one can expect this semi-empirical potential to also describe the longer-range correlations of the system reasonably well. More information about this strategy and an application on the Al and Al–Mg systems can be found elsewhere [32]. Here, we apply this method on the $Al_{90}Sm_{10}$ system. A semi-empirical potential in the Finnis–Sinclar (FS) format [34] is developed by fitting to a series of structural and thermodynamic quantities from first-principles calculations, such as the AIMD PPCFs of $Al_{90}Sm_{10}$ liquids, and the lattice constants and formation energies of several Al–Sm compounds. In figure 1, the solid lines show the PPCFs calculated by the classical MD calculations with the FS potential fitted to AIMD PPCFs up to a cut-off radius $r_c = 10.6$ Å. A much larger system containing 5000 atoms/unit cell was used in the classical MD calculations to fully converge the PPCFs. As can been seen in figure 1, the PPCFs from classical MD match those from AIMD. The dashed red line in figure 2 gives the total $S(q)$ calculated from the elongated PPCFs at 1300 K. One can see that the elongation effectively eliminates the transformation ripples in the small q range. The corrected $S(q)$ in the small q range compares favorably with experiments, further justifying the elongation method.

Figure 3(a) shows the calculated total structure factor $S(q)$ at three different temperatures $T = 1300$, 1000, and 800 K. At 1300 K, which is above the melting point, a prepeak starts to develop at $q \sim 1.3$ Å^{-1} before the primary peak located at $q \sim 2.5$ Å^{-1}. The prepeak becomes more prominent as the temperature decreases. According to equation (1), the total structure factor $S(q)$ is a weight sum of the partial structure factors $S_{\alpha\beta}(q)$. To show which components contribute to the prepeak, we plot the total $S(q)$ together with the weighted partials at a deeply undercooled temperature 800 K in figure 4. It is clearly seen that the prepeak is aligned with the first peak of the weighted partial $\omega_{22}S_{22}$, as indicated by the red arrow in figure 4. At the same time, $\omega_{11}S_{11}$ makes a negligible contribution to the prepeak, and $\omega_{12}S_{12}$ has a valley located close to the prepeak, thus working to annihilate the prepeak. Because the partial structure factor S_{22} is determined by the Sm–Sm pair correlation function $g_{22}(r)$, we can come to the conclusion that the prepeak in $Al_{90}Sm_{10}$ liquids and undercooled liquids are both originated from the Sm–Sm correlations in the system. Figure 3(b) shows the Sm–Sm PPCFs produced by AIMD calculations at various temperatures. The intensity of all major peaks increases as the temperature decreases, demonstrating enhanced structural ordering as the liquid becomes more deeply undercooled. Furthermore, a unique feature of $g_{22}(r)$ up to the medium range at all temperatures is that the first peak is decisively weaker than the second one. Because the short to medium range correlations are the most fundamental components of the Sm–Sm pair correlation function, we believe that the relative

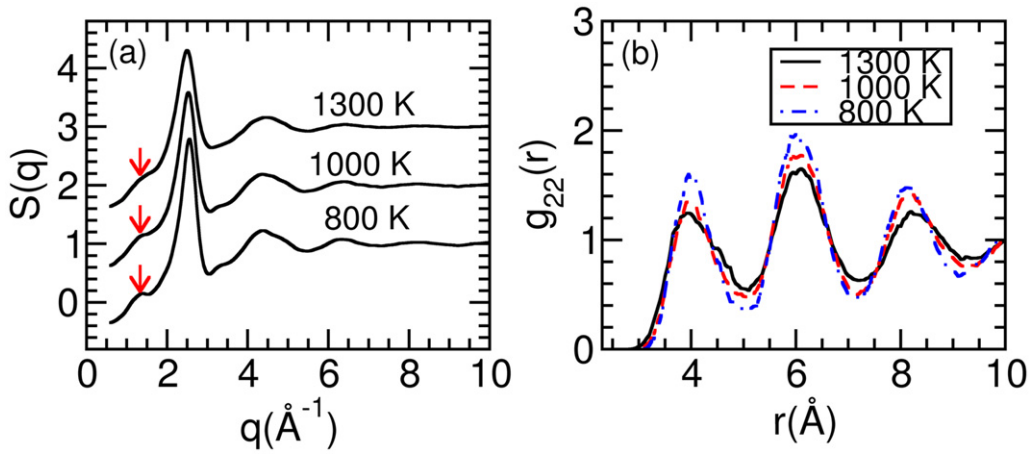

Figure 3. (*a*) Total structure factor of the $Al_{90}Sm_{10}$ system at various temperatures, calculated by AIMD with the elongation method. The arrows indicate the position of the prepeak. (*b*) Sm–Sm PPCF at various temperatures from pure AIMD calculations.

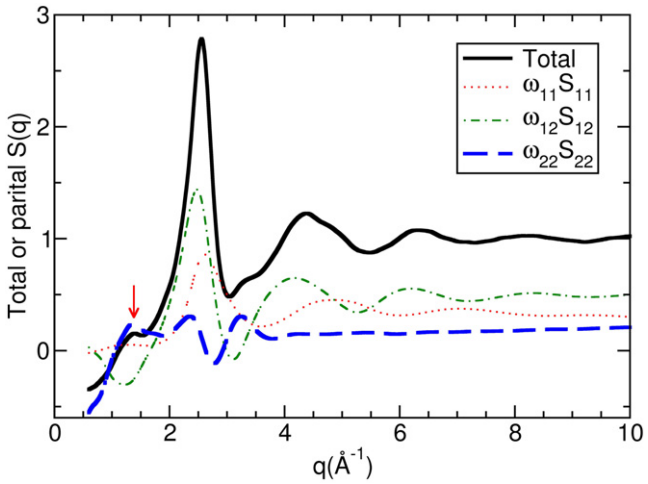

Figure 4. Total structure factor and its weighted components of the $Al_{90}Sm_{10}$ system at $T = 800$ K. The prepeak in the total $S(q)$ lines up with a peak in $\omega_{22}(q)S_{22}(q)$, as indicated by an arrow.

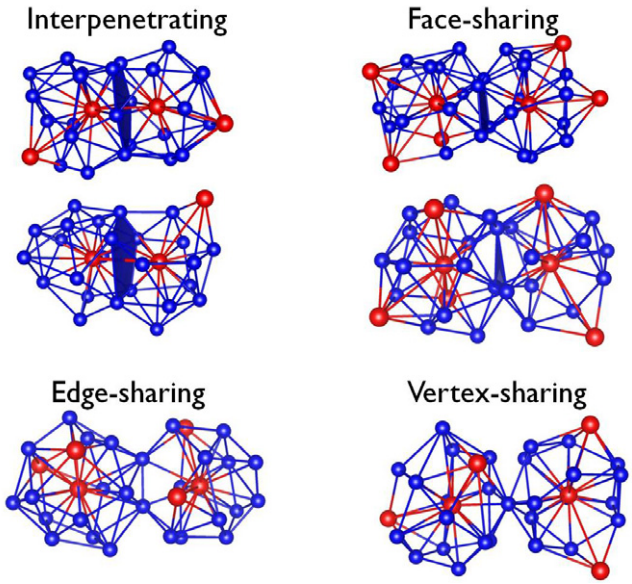

Figure 5. Different connection types of two adjacent Sm-centered clusters in AIMD samples of $Al_{90}Sm_{10}$ at $T = 800$ K. Interpenetrating: two clusters share a hexagonal or pentagonal bipyramid (one Sm is on the first shell of the cluster surrounding the other). Face-sharing: two clusters share a square of the triangular Al face. Edge-sharing: two clusters share a nearest-neighboring Al pair. Vertex-sharing: two clusters share a single Al atom.

strength of the first two peaks plays an essential role to give rise to the prepeak in the total $S(q)$.

We now analyze what structural units are associated with the Sm–Sm PPCF, where the first peak is lower than the second one. Recently, we have studied the SRO of the $Al_{90}Sm_{10}$ system, which is characterized by solute (Sm)-centered clusters due to the large affinity between Al and Sm atoms [33]. Because Sm has a significantly larger atomic size than Al, the Sm-centered clusters have large coordination numbers (>15) and commonly contain pentagonal or hexagonal Al rings on the first shell [33]. These high-member Al rings create a large empty space to accommodate a Sm dimer, i.e. two neighboring Sm atoms whose separation is close enough to contribute to the first peak of $g_{22}(r)$, forming a bipyramidal local structure. The bipyramid is shared by the two clusters surrounding Sm atoms on both ends, resulting in interpenetrating connection of the two Sm-centered clusters, as shown in figure 5(*a*). To identify other possible connection types between two Sm-centered clusters that characterize the short-range order of the system [33], we have systematically analyzed the number of common neighbors based on a cut-off separation of 4.3 Å. The cut-off value is determined based on the position of the first minimum of the Al–Sm partial pair correlation function (figure 1), because each Sm is surrounded predominantly by Al atoms. In addition to the interpenetrating connection, two Sm-centered clusters can also share a square or triangular face (figure 5(*b*)). In such cases, the separation of the two center Sm atoms in general exceeds the range of the first peak of the Sm–Sm pair correlation function. With further increasing Sm–Sm separations, two adjacent Sm-centered clusters can also be connected by sharing a edge or a vertex, as shown in figures 5(*c*) and (*d*), respectively.

Figure 6(*a*) shows the probability distribution of the Sm–Sm separation for the four connection types discussed in the

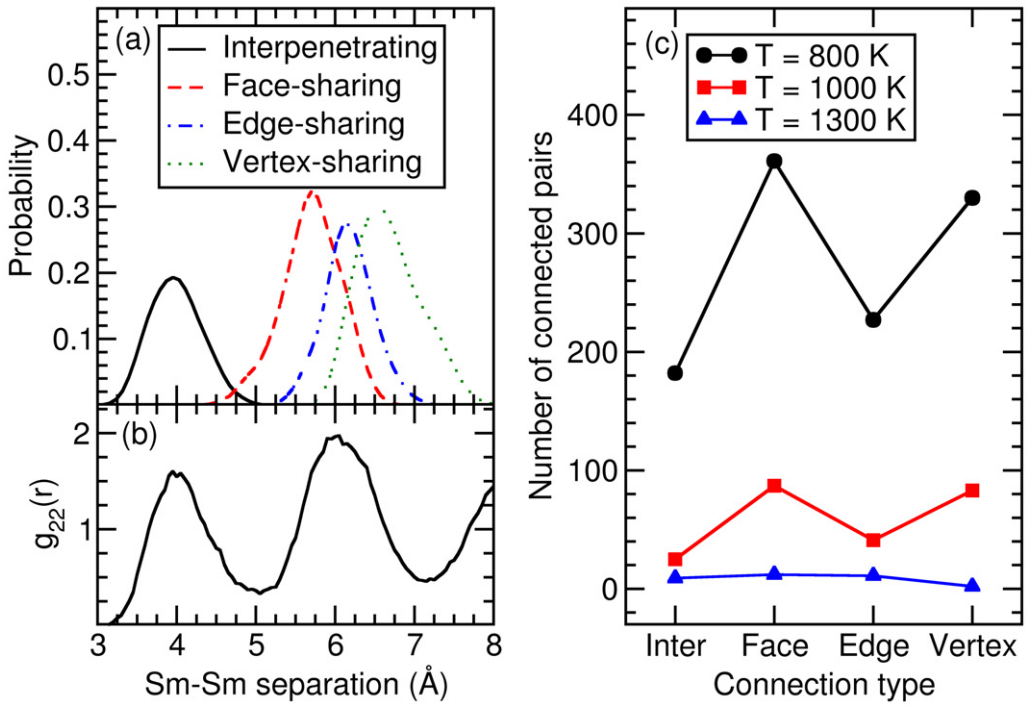

Figure 6. (*a*) The probability distribution of the Sm–Sm separation for each connection type of two adjacent Sm-centered clusters. (*b*) The Sm–Sm pair correlation function for the AIMD $Al_{90}Sm_{10}$ sample at 800 K. (*c*) The number of connected Sm-centered pairs in each connection type at various temperatures. In (*a*), the area of each distribution function is equal to the fraction of the corresponding connection type; thus, the sum of the areas of the four distribution functions is equal to 1.

AIMD sample at $T = 800$ K. The area of each distribution function is equal to the fraction of the corresponding connection type (the sum of the areas of the four distributions is equal to 1). One can see that only the interpenetrating connection contributes to the first peak of $g_{22}(r)$ (figure 6(*b*)), whereas all three other connection types contribute to the second peak. Moreover, the interpenetrating connection is less favorable than other connection types, probably because of the intrinsic repulsion between Sm atoms. However, the interpenetrating connection cannot be completely annihilated due to the large space created by the pentagonal or hexagonal Al rings in the system. On the contrary, as the temperature decreases, the fraction of the interpenetrating connection grows, as can be seen in figure 6(*c*). The same trend is also evidenced by the increasing intensity of the first peak in $g_{22}(r)$ shown in figure 3(*b*). This is consistent with the enhancement of the SRO containing pentagonal and hexagonal Al rings, as the liquid becomes more deeply undercooled [33]. These factors collectively give the overall shape of $g_{22}(r)$ with a stronger second peak, which in turn gives the prepeak in the total $S(q)$.

Finally, we demonstrate that the large AIMD model containing 500 atoms is necessary to reliably capture the Sm–Sm correlations. Because the AIMD relaxation of the 500-atom model is computationally expensive, one would wonder whether a smaller model is sufficient to study the structure. For example, in a 200-atom model, the PPCFs can be calculated up to ∼8 Å. In some cases, like the $Al_{50}Mg_{50}$ alloy considered elsewhere [32], such a small model would be sufficient. However, another difficulty in study of the $Al_{90}Sm_{10}$ alloy is associated with the fact that the Sm fraction is very small, and a 200-atom model contains only 20 Sm atoms. Taking into account a rather short time available for averaging in the AIMD simulation, it is not obvious that such a small model will include all possible structural units of the alloy under consideration. Figures 7(*a*)–(*c*) shows an example of PPCFs obtained from a model containing 200 atoms using the same MD procedure as was used for the model with 500 atoms. Although Al–Al and Al–Sm PPCFs can be reliably extracted from a smaller model, the Sm–Sm PPCF is considerably different than that obtained using a larger model. In particular, for the 200-atom model, the first peak is significantly stronger than the second one. Applying exactly the same elongation procedure to these PPCFs we obtained the structure factor that does not show the prepeak, as can been seen from figure 7(*d*).

4. Conclusion

In summary, we studied a typical system formed by Al and 10 at.% Sm using *ab initio* molecular dynamics within the density-functional theory. The unit cell contains 500 atoms, which is large enough to capture the Sm–Sm correlation up to the medium range in the system, which eventually produces a profound prepeak in the structure factor of the system. The prepeak emerges in the liquid state, and becomes more prominent as the temperature decreases to the undercooled regime. The calculated structure factor agrees well with x-ray diffraction experiments. The Sm–Sm correlation is determined by the networking of Sm-centered clusters, which reflects the medium-range order of the system. The connection of adjacent

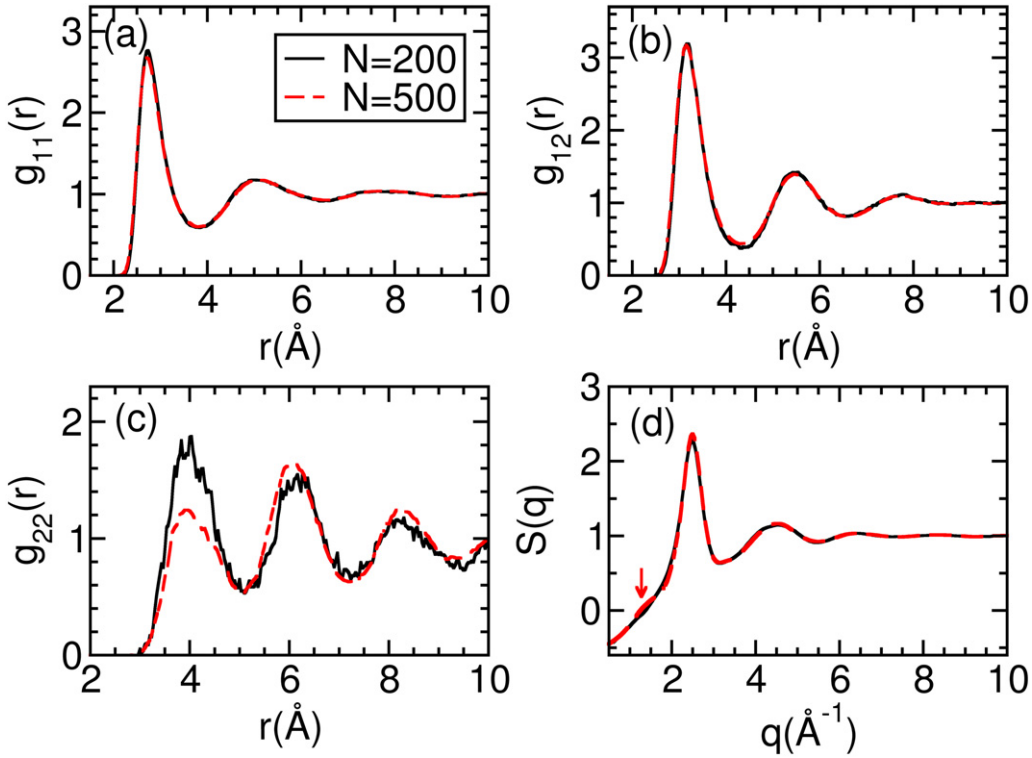

Figure 7. (*a*)–(*c*) Partial pair correlation functions of $Al_{90}Sm_{10}$ at $T = 1300$ K, calculated on two samples with different numbers of atoms per unit cell. (*d*) The total structure factor for the two samples. The red arrow indicates the emergence of a prepeak in the $N = 500$ sample.

Sm-centered clusters is affected by two factors. First, high-member Al rings commonly existing in the system open up large space for neighboring Sm pairs. Second, the intrinsic repulsion pushes Sm atoms to larger separations. As a result, the interpenetrating connection of two Sm-centered clusters exists, but it is less favorable than other connection types, including face-sharing, edge-sharing, and vertex-sharing. In turn, the Sm–Sm pair correlation function has a stronger second peak than the first one. This unique profile of Sm–Sm correlation eventually produces the prepeak in the structure factor.

Acknowledgments

Work at Ames Laboratory was supported by the US Department of Energy, Basic Energy Sciences, Division of Materials Science and Engineering under Contract No. DE-AC02-07CH11358, including a grant of computer time at the National Energy Research Supercomputing Center (NERSC) in Berkeley, CA.

References

[1] Inoue A 1998 *Prog. Mater. Sci.* **43** 365
[2] Inoue A, Ohtera K, Tao Z and Masumoto T 1988 *Japan. J. Appl. Phys.* **2** L1583
[3] He Y, Poon S J and Shiflet G J 1988 *Science* **241** 1640
[4] Kim Y H, Inoue A and Masumoto T 1991 *Mater. Trans. JIM* **32** 331
[5] Zhong Z C, Jiang X Y and Greer A L 1997 *Mater. Sci. Eng.* A **226** 531
[6] Rizzi P, Antonione C, Baricco M, Battezzati L, Armelao L, Tondello E, Fabrizio M and Daolio S 1998 *Nanostruct. Mater.* **10** 767
[7] Zhou S H and Napolitano R E 2007 *Metall. Mater. Trans.* A **38A** 1145
[8] Kalay Y E, Yeager C, Chumbley L S, Kramer M J and Anderson I E 2010 *J. Non-Cryst. Solids* **356** 1416
[9] Cheng Y Q and Ma E 2011 *Prog. Mater. Sci.* **56** 379
[10] Frank F 1952 *Proc. R. Soc.* A **215** 43
[11] Hsieh H Y, Toby B H, Egami T, He Y, Poon S J and Shiflet G J 1990 *J. Mater. Res.* **5** 2807
[12] Hsieh H Y, Egami T, He Y, Poon S J and Shiflet G J 1991 *J. Non-Cryst. Solids* **135** 248
[13] Zhang L, Wu Y, Bian X, Li H, Wang W, Li J and Lun N 1999 *J. Phys.: Condens. Matter* **11** 7959
[14] Saksl K, Jóvári P, Franz H and Jiang J Z 2005 *J. Appl. Phys.* **97** 113507
[15] Karel S, Pál J, Hermann F, Zeng Q S, Liu J F and Jiang J Z 2006 *J. Phys.: Condens. Matter* **18** 7579
[16] Ahn K, Louca D, Poon S J and Shiflet G J 2004 *Phys. Rev.* B **70** 224103
[17] Kalay Y E, Chumbley L S, Kramer M J and Anderson I E 2010 *Intermetallics* **18** 1676
[18] Elliott S R 1991 *Nature* **354** 445
[19] Susman S *et al* 1991 *Phys. Rev.* B **43** 1194
[20] Wilson M and Madden P 1994 *Phys. Rev. Lett.* **72** 3033
[21] Cobb M, Drabold D A and Cappelletti R L 1996 *Phys. Rev.* B **54** 12162
[22] Salmon P S, Martin R A, Mason P E and Cuello G J 2005 *Nature* **435** 75
[23] Massobrio C and Pasquarello A 2008 *Phys. Rev.* B **77** 144207
[24] Wilson M and Salmon P 2009 *Phys. Rev. Lett.* **103** 157801
[25] Kresse G and Furthmüller J 1996 *Comput. Mater. Sci.* **6** 15
[26] Kresse G and Joubert D 1999 *Phys. Rev.* B **59** 1758
[27] Perdew J P, Burke K and Ernzerhof M 1996 *Phys. Rev. Lett.* **77** 3865

[28] Martyna G J, Klein M L and Tuckerman M 1992 *J. Chem. Phys.* **97** 2635
[29] Okamoto H 2012 *J. Phase Equilib. Diffus.* **33** 243
[30] Faber T E and Ziman J M 1965 *Phil. Mag.* **11** 153
[31] Waasmaier D and Kirfel A 1995 *Acta. Crystallogr.* A **51** 416
[32] Kramer M J, Mendelev M I and Asta M 2014 *Phil. Mag.* **94** 1876
[33] Sun Y *et al* 2014 at press (arXiv:1408.1714)
[34] Finnis M and Sinclair J 1984 *Phil. Mag.* A **50** 45